LOS and NLOS Classification for Underwater Acoustic Localization

Roee Diamant*, Hwee-Pink Tan† and Lutz Lampe*

*Electrical and Computer Engineering, The University of British Columbia

†Institute for Infocomm Research, Singapore

Email: {roeed,lampe}@ece.ubc.ca and hptan@i2r.a-star.edu.sg

Abstract

The low sound speed in water makes propagation delay (PD) based range estimation attractive for underwater acoustic localization (UWAL). However, due to the long channel impulse response and the existence of reflecting objects, PD-based UWAL suffers from significant degradation when PD measurements of non-line-of-sight (NLOS) communication links are falsely identified as line-of-sight (LOS) communication links. In this paper, we present an algorithm to classify PD measurements into LOS and NLOS links for a single transmitter-receiver pair. First, by comparing signal strength-based and PD-based range measurements, we identify object-related NLOS (ONLOS) links, where signals are reflected from objects with high reflection loss, e.g., ships hull, docks, rocks, etc. In the second step, excluding PD measurements related to ONLOS links, we use a constrained expectation-maximization algorithm to classify PD measurements into two classes: LOS and sea-related NLOS (SNLOS), and to estimate the statistical parameters of each class. Since our classifier relies on models for the underwater acoustic channel, which are often simplified, alongside simulation results, we validate the performance of our classifier based on measurements from three sea trials. Both our simulation and sea trial results demonstrate a high detection rate of ONLOS links, and accurate classification of PD measurements into LOS and SNLOS.

Index Terms

Underwater acoustic localization (UWAL), line-of-sight, non-line-of-sight, time-of-arrival classification.

Parts of this work have been presented at the IEEE Oceans Conference, Sep. 2010, Seattle, USA.

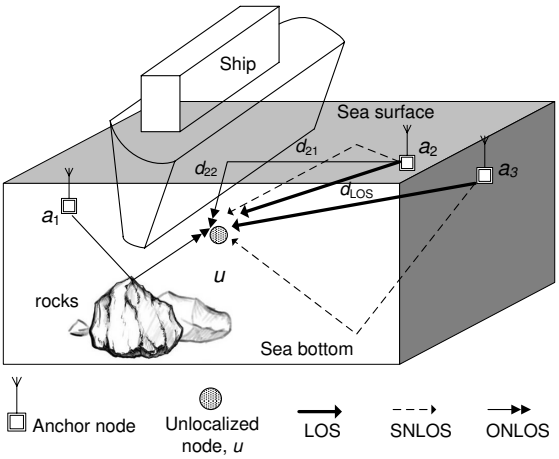

Fig. 1: Illustration of various types of communication links: LOS, SNLOS and ONLOS links.

I. Introduction

Underwater acoustic communication networks (UWAN) are envisaged to fulfill the needs of a multitude of applications such as navigation aids, early warning systems for natural disasters, ecosystem monitoring and military surveillance [1]. The data derived from UWAN is typically interpreted with reference to a node's location, e.g., reporting an event occurrence, tracking a moving object or monitoring a region's physical conditions. However, localization for underwater nodes is non-trivial. Since GPS signals do not propagate through water, localization of unlocalized nodes is often based on underwater acoustic communication and triangulation using a set of anchor nodes with known locations. This underwater acoustic localization (UWAL) typically employs propagation delay (PD) measurements for range estimation, i.e., time of arrival (ToA) or time difference of arrival (TDoA) of received signals [2], since angle of arrival methods would require multiple hydrophones and signal-strength based methods would fail due to inaccurate propagation models.

Existing UWAL schemes, e.g., [3], [4], [5], implicitly assume that PD measurements correspond to the line-of-sight (LOS) link between the transmitter and receiver. However, signals can arrive from non-LOS (NLOS) communication links in several ways, as illustrated in Figure 1. For the node pairs (u, a_2) and (u, a_3), sea surface and bottom reflections links (referred to as sea-related NLOS (*SNLOS*)) exist, respectively, in addition to an LOS link. For (u, a_1), the signal

arrives from the reflection off a rock (referred to as object-related NLOS (*ONLOS*)). Lastly, between nodes u and a_2, there is also an ONLOS link due to a ship. While it is expected that power attenuation in the LOS link is smaller than in NLOS links, it is common that the LOS signal is not the strongest. This is because, as shown in multipath models [6] as well as measurements [7], the underwater acoustic channel (UWAC) consists of groups of NLOS links with small path delay, but significant phase differences, often resulting in negative superposition with the LOS link (if delay differences between the LOS and NLOS links are smaller than the system resolution for path separation) as well as positive superposition between NLOS links. If PD measurements of NLOS links are mistakenly treated as corresponding to delay in the LOS link, e.g., in node pairs (u, a_2) and (u, a_3), localization accuracy will significantly be degraded.

In this paper, we propose a two-step algorithm to classify a vector of PD measurements for a single transmitter-receiver distance into three classes: **LOS**, **SNLOS** and **ONLOS**, which is a problem that has not been treated in previous literature. Such a classification can improve the accuracy of UWAL by either rejecting NLOS-related PD measurements, correcting them, or using them to bound range estimation. We first identify ONLOS-related PD-measurements by comparing PD-based range estimations with range estimations obtained from received-signal-strength (RSS) measurements. Considering the difficulty in acquiring an accurate attenuation model, our algorithm requires only a lower bound for RSS-based distance estimations. After excluding PD measurements related to ONLOS, we apply a constrained expectation-maximization (EM) algorithm to further classify the remaining PD measurements into LOS and SNLOS, and estimate the statistical parameters of both classes to improve the accuracy of UWAL. Results from extensive simulations and three sea trial experiments in different areas of the world demonstrate the efficacy of our approach through achieving a high detection rate for ONLOS links and good classification of non-ONLOS related PD measurements into LOS and SNLOS.

It should be noted that while our approach can also be adapted to other types of fading channels, it is particularly suited for UWAL for the following reasons. First, our algorithm relies on significant power absorption due to reflection loss in ONLOS links, which are typical in the underwater environment. Second, we assume that the difference in propagation delay between signals traveling through SNLOS and LOS links is noticeable, which is acceptable in the UWAC due to the low sound speed in water (approximately 1500 m/sec). Third, our algorithm is particularly beneficial in cases where NLOS paths are often mistaken for the LOS path, which

occurs in UWAL, where the LOS path is frequently either not the strongest or non-existent. Last, we assume that the variance of PD measurements originating from SNLOS links is greater than that of measurements originating from LOS, which fits channels with long delay spread such as the UWAC.

The remainder of this paper is organized as follows. Related work on PD-based underwater localization is described in Section II. Our system model and assumptions are introduced in Section III. In Section IV, we present our approach to identify ONLOS links. Next, in Section V, we formalize the EM algorithm to classify non-ONLOS related PD measurements into LOS and SNLOS. Section VI includes performance results of our two-step algorithm obtained from synthetic UWAC environments (Section VI-A) and from three different sea trials (Section VI-B). Finally, conclusions are offered in Section VII. The key notations used in this paper are summarized in Table I.

TABLE I: List of key notations

Notation	Explanation
x_i	PD measurements
$\boldsymbol{X}$	vector of PD measurements x_i of the same communication link
d	transmission distance
d^{PD}	PD-based range estimation
$d^{\mathrm{RSS,min}}$	lower bound of RSS-based range measurement
γ	propagation loss factor
$\gamma_{\max}$	upper bound for γ
α	absorption loss factor
M	assumed number of classes in PD model
k_m	weight of the mth distribution in the mixture distribution model
$\boldsymbol{\omega}_m = [\upsilon_m, \sigma_m, \beta_m]$	vector of parameters of the mth distribution
$\boldsymbol{\theta}$	vector of parameters of the distribution of $\boldsymbol{X}$
T_{LIR}	upper bound on the length of the channel impulse response
c	propagation speed in the channel
$x_{\mathrm{LOS}},\ d_{\mathrm{LOS}}$	delay and distance in the LOS link, respectively
d_{ONLOS}	distance of the ONLOS link
RL	reflection loss in ONLOS link
$\boldsymbol{x}_l$	group of x_i measurements with the same distribution $\boldsymbol{\omega}_m$
λ_l	classifier for group $\boldsymbol{x}_l$
ϱ_i	classifier for x_i

II. Related Work

PD measurements for range estimation can be obtained (i) from the symbols of a received data packet or (ii) from multiple impulse-type signals transmitted in a short period of time. The former is a standard in many ultra short baseline systems (e.g., [8]) and involves inspecting the output of an energy detector [9]. The latter involves inspecting the estimated channel impulse response by performing a matched filter operation at the receiver [7], or by performing a phase-only correlation and using the kurtosis metric to mitigate channel enhanced noise [10]. The PD is then estimated by setting a detection threshold to identify the arrival of the first path. In [11], a fixed threshold is set based on the channel noise level and a target false alarm probability. In [12], an adaptive threshold is used based on the energy level of the strongest path. A good overview of practical PD estimators is given in [9].

Mistaking NLOS links for the LOS link gives rise to ranging errors which are usually regarded as part of the measurement noise [13]. In [14], direct sequence spread spectrum (DSSS) signals, which have narrow auto-correlation, are transmitted to allow better separation of paths in the estimated channel response. Following this approach, curve fitting of ToA measurements based on DSSS was suggested in [15]. Averaging ToA measurements from different signals is suggested in [16], where results show considerable reduction in measurement errors. In [3], NLOS-related noise for UWAC is modeled using the Ultra Wideband Saleh-Valenzuela (UWB-SV) model [17], and a method for mitigating multipath noise for a given multipath model was introduced in [18].

Several works suggested methods to compensate for location ambiguities such as flips and rotations that arise due to NLOS-related range estimation errors. In [19], additional anchor nodes were used to resolve such ambiguities. In [20], a three-phase protocol is suggested for this problem. First, an ambiguity-free sub-tree of nodes is determined. Then, localization based on triangulation is performed where the node is first assumed to be located in the center of a rectangular area. Finally, a refinement phase is performed using a Kalman filter to mitigate noise arising from ranging. A robust protocol for mitigating localization ambiguities is suggested in [21] by rejecting measurements leading to ambiguities, e.g., when there are insufficient anchor nodes or when the location of anchor nodes is almost collinear. The problem of localization when all measurements are obtained from NLOS links is considered in [22], where the relationship between anchor node distances and NLOS factor is used to improve localization. However, these

protocols are only applicable when a large number of anchor nodes are available.

Associating PD measurements with LOS or NLOS can improve localization accuracy. In [23], measurements which increase the global variance are rejected, assuming that NLOS-based measurements have larger variance than LOS-based measurements. In [24], localization accuracy is improved by selecting ToA measurements based on minimal statistical mode (i.e., minimal variance and mean). Alternatively, the authors in [25] suggested a method for reducing the effect of NLOS-based noise by assigning each measurement with a weight inversely proportional to the difference between the measured and expected distances from previous localization. In [26], an NLOS factor (i.e., the difference between the arrival times of the NLOS and LOS-based signals) is estimated using a maximum likelihood estimator based on an attenuation model, and NLOS-based measurements are incorporated after a factor correction instead of being rejected. However, to the best of our knowledge, no prior work considered NLOS and LOS classification of PD measurements for the special characteristics of the UWAC.

III. System Setup and Assumptions

Referring to Figure 1, our system comprises of one or more transmitter-receiver pairs, (u, a_j), exchanging a single communication packet of N symbols or impulse signals, from which a vector $\boldsymbol{X} = [x_1, \ldots, x_N]$ of PD measurements x_i, is obtained using detectors such as in, e.g., [8], [7], [10]. We model x_i such that

$$x_i = x_{\text{LOS}} + n_i \ , \tag{1}$$

where x_{LOS} is the transmitter-receiver PD in the LOS link, assumed to be fixed during the time $\boldsymbol{X}$ is obtained[1], and n_i is zero-mean (for LOS links) or non-zero-mean (for SNLOS or ONLOS links) measurement noise. We assume signals are separated by guard intervals such that n_i are i.i.d. Each measurement x_i corresponds to a measured time t_i, and a PD-based estimate, d_i^{PD}, is obtained by multiplying x_i with an assumed propagation speed, c. In addition, based on an attenuation model for an LOS link, we obtain RSS-based range estimates, $d_i^{\text{RSS}},\ i = 1, \ldots, N$, from the received signals.

In the following, we introduce our system model for obtaining RSS-based range measurements as well as the assumed probability density function (PDF) for PD measurements.

[1]A relaxation of this assumption is presented further below.

A. RSS-Based Range Measurements

Let d_{LOS} denote the distance corresponding to x_{LOS}, i.e., $d_{\mathrm{LOS}} = x_{\mathrm{LOS}}c$. For the purpose of obtaining RSS-based range measurements, we use the popular model [27]

$$\mathrm{TL}_{\mathrm{LOS}}(d_{\mathrm{LOS}}) = \mathrm{PL}(d_{\mathrm{LOS}}) + \mathrm{AL}(d_{\mathrm{LOS}}) + \epsilon \ , \tag{2}$$

where $\mathrm{PL}(d_{\mathrm{LOS}}) = \gamma \log_{10}(d_{\mathrm{LOS}})$ is the propagation loss, $\mathrm{AL}(d_{\mathrm{LOS}}) = \alpha \frac{d_{\mathrm{LOS}}}{1000}$ is the absorption loss, γ and α are the propagation and absorption coefficients, respectively, and ϵ is the model noise assumed to be Gaussian distributed with zero mean and variance ϕ. Considering the simplicity of the model in (2), we do not directly estimate d_i^{RSS} but rather estimate a lower bound $d_i^{\mathrm{RSS,min}}$, for which we apply upper bounds for γ and α in (2) according to the expected underwater environment.

For an ONLOS link with distance $d_{\mathrm{ONLOS}} = d_{\mathrm{ONLOS},1} + d_{\mathrm{ONLOS},2}$, where $d_{\mathrm{ONLOS},1}$ and $d_{\mathrm{ONLOS},2}$ are the distance from source to reflector and from reflector to receiver, respectively[2], we assume that the power attenuation in logarithmic scale is given by [27]

$$\mathrm{TL}_{\mathrm{ONLOS}}(d_{\mathrm{ONLOS}}) = \mathrm{TL}_{\mathrm{LOS}}(d_{\mathrm{ONLOS},1}) + \mathrm{TL}_{\mathrm{LOS}}(d_{\mathrm{ONLOS},2}) + \mathrm{RL} \ , \tag{3}$$

where RL is the reflection loss of the reflecting object. We further assume that RL, which depends on the material and structure of the object and the carrier frequency of the transmitted signals, is sufficiently large such that

$$\mathrm{TL}_{\mathrm{ONLOS}}(d_{\mathrm{ONLOS}}) \gg \mathrm{TL}_{\mathrm{LOS}}(d_{\mathrm{ONLOS}}) \ . \tag{4}$$

B. PDF for PD Measurements

We model the PDF of the noisy measurement x_i as a mixture of $M = 3$ distributions, corresponding to LOS, SNLOS, and ONLOS links, such that (assuming independent measurement noise samples in (1))

$$p(\boldsymbol{X}|\boldsymbol{\theta}) = \prod_{x_i \in \boldsymbol{X}} \sum_{m=1}^{M} k_m p(x_i|\boldsymbol{\omega}_m) \ , \tag{5}$$

where $\boldsymbol{\theta} = [\boldsymbol{\omega}_1, k_1, \ldots, \boldsymbol{\omega}_M, k_M]$, $\boldsymbol{\omega}_m$ are the parameters of the mth distribution, and k_m ($\sum_{m=1}^{M} k_m = 1$) is the a-priori probability of the mth distribution. Clearly, $p(\boldsymbol{X}|\boldsymbol{\theta})$ depends on

[2]Referring to the ONLOS link between node pair (u, a_2) in Figure 1, $d_{\mathrm{ONLOS},1} = d_{21}$ and $d_{\mathrm{ONLOS},2} = d_{22}$.

both the UWAC and the detector used to estimate x_i. While recent works used the Gaussian distribution for $p(x_i|\boldsymbol{\omega}_m)$ (cf., [28] and [29]), we take a more general approach and model it according to the generalized Gaussian PDF [30], such that

$$p(x_i|\boldsymbol{\omega}_m) = \frac{\beta_m}{2\sigma_m \Gamma\left(\frac{1}{\beta_m}\right)} e^{-\left(\frac{|x_i - \upsilon_m|}{\sigma_m}\right)^{\beta_m}} \tag{6}$$

with parameters $\boldsymbol{\omega}_m = [\beta_m, \upsilon_m, \sigma_m]$. We associate the parameter vectors $\boldsymbol{\omega}_1$, $\boldsymbol{\omega}_2$, and $\boldsymbol{\omega}_3$ with distributions corresponding to the LOS, SNLOS, and ONLOS links, respectively. Thus, by (1), $\upsilon_1 = x_{\text{LOS}}$. The use of parameter β_m in (6) gives our model a desired flexibility, with $\beta_m = 1$, $\beta_m = 2$, and $\beta_m \to \infty$ corresponding to Laplace, Gaussian, and uniform distribution, respectively. The flexibility and fit of model (6) is demonstrated using sea trial results in Section VI-B.

Following [23] and [24], we assume that PD measurements of NLOS links increase the variance of the elements of $\boldsymbol{X}$. Thus, if ς_1, ς_2, and ς_3 are the respective variances of measurements related to the LOS, SNLOS, and ONLOS links, then we have

$$\varsigma_1 < \varsigma_m, \ m = 2, 3. \tag{7}$$

Since, for the PDF (6),

$$\varsigma_m = (\sigma_m)^2 \frac{\Gamma\left(\frac{3}{\beta_m}\right)}{\Gamma\left(\frac{1}{\beta_m}\right)}, \tag{8}$$

and by (8), ς_m does not change much with β_m, constraint (7) can be modified to

$$\sigma_1 < \sigma_m, \ m = 2, 3. \tag{9}$$

Furthermore, let T_{LIR} be the assumed length of the UWAC impulse response, which is an upper bound on the time difference between the arrivals of the last and first paths. Then, since ς_1, ς_2, and ς_3 in (8) capture the spread of measurements related to the LOS, SNLOS, and ONLOS links respectively,

$$\sqrt{\varsigma_m} < T_{\text{LIR}}, \ m = 1, 2, 3 \, . \tag{10}$$

Moreover, the propagation delay through the LOS link is almost always shorter than those for

any NLOS link[3]. Hence, we have

$$\upsilon_1 < \upsilon_m < \upsilon_1 + T_{\mathrm{LIR}},\ m = 2, 3. \tag{11}$$

C. Remark on Algorithm Structure

We offer a two-step approach to classify PD measurements into LOS, SNLOS, and ONLOS. First, assuming large attenuation in an ONLOS link, we compare PD-based and RSS-based range estimates to differentiate between ONLOS and non-ONLOS links. Then, assuming PDF (6) for PD measurements, we further classify non-ONLOS links into LOS and SNLOS links. We thus exploit in the first step that d_i^{RSS} is significantly different for ONLOS compared to LOS and SNLOS links. This in turn simplifies classification in the second step, which is based on the estimation of statistical parameters using (6). In the following sections, we describe our two-step approach for classifying PD measurements.

IV. Step One: Identifying ONLOS Links

Considering (4), we identify whether measurement $x_i \in \boldsymbol{X}$ is ONLOS-related based on three basic steps as follows:

- **Estimation of** d_i^{PD}
  We first obtain the PD-based range estimation as $d_i^{\mathrm{PD}} = c \cdot x_i$.
- **Estimation of** $d_i^{\mathrm{RSS,min}}$
  Next, assuming knowledge of the transmitted power level, we measure the RSS for the ith received signal/symbol, and estimate $d_i^{\mathrm{RSS,min}}$ based on (2), replacing γ and α with upper bounds $\gamma_{\max}$ and $\alpha_{\max}$, respectively.
- **Thresholding**
  Finally, we compare d_i^{PD} with $d_i^{\mathrm{RSS,min}}$. If $d_i^{\mathrm{RSS,min}} > d_i^{\mathrm{PD}}$, then x_i is classified as ONLOS. Otherwise, it is determined as non-ONLOS.

Next, we analyze the expected performance of the above ONLOS link identification algorithm in terms of (i) detection probability of non-ONLOS links, $\mathrm{Pr}_{\mathrm{d,non-ONLOS}}$, and (ii) detection

[3]We note that in some UWACs, a signal can propagate through a soft ocean bottom, in which case SNLOS signals may arrive before the LOS signal [27]. However, such scenarios are not considered in this work.

probability of ONLOS links, $\mathrm{Pr}_{\mathrm{d,ONLOS}}$. To this end, since explicit expression for d_{LOS} cannot be obtained from (2), in the following, we use the upper bound $\tilde{d}^{\mathrm{RSS,min}}$ such that

$$\log_{10}(\tilde{d}^{\mathrm{RSS,min}}) = \frac{\mathrm{TL}}{\gamma_{\max}} \,. \tag{12}$$

We note that (12) is a tight bound when the carrier frequency is low or when the transmission distance is small.

A. Classification of non-ONLOS links

For non-ONLOS links, we expect $d_i^{\mathrm{RSS,min}} \leq d_{\mathrm{LOS}}$. Thus, since by bound (12), $\Pr(d_i^{\mathrm{RSS,min}} \leq d_{\mathrm{LOS}}) \geq \Pr(\tilde{d}_i^{\mathrm{RSS,min}} \leq d_{\mathrm{LOS}})$, and substituting (2) in (12), we get

$$\mathrm{Pr}_{\mathrm{d,non-ONLOS}} \geq 1 - Q\left(\frac{(\gamma_{\max} - \gamma)\log_{10}(d_{\mathrm{LOS}}) - \alpha\frac{d_{\mathrm{LOS}}}{1000}}{\phi}\right) \,, \tag{13}$$

where $Q(x)$ is the Gaussian Q-function.

B. Classification of ONLOS links

When the link is ONLOS, we expect $d_i^{\mathrm{RSS,min}} \geq d_{\mathrm{ONLOS}}$. Then, substituting (3) in (12), and since $\Pr(d_i^{\mathrm{RSS,min}} \geq d_{\mathrm{ONLOS}}) \leq \Pr(\tilde{d}_i^{\mathrm{RSS,min}} \geq d_{\mathrm{ONLOS}})$, we get

$$\mathrm{Pr}_{\mathrm{d,ONLOS}} \leq Q\left(\frac{\gamma_{\max}\log_{10}(d_{\mathrm{ONLOS}}) - \gamma\log_{10}(d_{\mathrm{ONLOS},1}d_{\mathrm{ONLOS},2}) - \alpha\frac{d_{\mathrm{ONLOS}}}{1000} - \mathrm{RL}}{\phi}\right) \,. \tag{14}$$

Next, we continue with classifying non-ONLOS links into LOS and SNLOS links.

V. Step 2: Classifying LOS and SNLOS Links

After excluding ONLOS-related PD measurements in Step 1, the remaining elements of $\boldsymbol{X}$, organized in the pruned vector $\boldsymbol{X}^{\mathrm{ex}}$, are further classified into LOS ($m = 1$) and SNLOS ($m = 2$) links and their statistical distribution parameters, $\boldsymbol{\omega}_m$, are estimated.

Recall that estimations x_i correspond to measurement times t_i. Assuming that the channel impulse response is constant within a coherence time, T_c, and that for a bandwidth B of the transmitted signal system resolution is limited by $\Delta T = \frac{1}{B}$, we can set *equivalence* constraints such that closely spaced measurements are classified into the same class. PD measurements satisfying equivalence constraints are collected into vectors $\boldsymbol{x}_l,\ l = 1, \ldots, L$, where L denotes the number of such equivalence sets. Each PD measurement is assigned to exactly one vector,

i.e., $\boldsymbol{x}_l$ have distinct elements. To formalize this, we determine x_i and x_j being equivalent, denoted as $x_i \Leftrightarrow x_j$, if

$$|t_i - t_j| \leq T_c \tag{15a}$$

$$|x_i - x_j| \leq \Delta T \ . \tag{15b}$$

Furthermore, while we assume in (1) that x_{LOS} is constant for the time period during which vector $\boldsymbol{X}$ is obtained, nodes may actually slightly move during that time[4], and such motion can affect the distribution of PD measurements of the same class. To illustrate this, let x_i, x_j, and x_n correspond to the same class (either LOS or NLOS), such that $x_i \Leftrightarrow x_j$ and $x_j \Leftrightarrow x_n$. Due to node motions, condition (15b) might not be satisfied for the pair x_i and x_n. Accounting for such motions, we construct vectors $\boldsymbol{x}_l$ such that if $x_i \Leftrightarrow x_j$ and $x_j \Leftrightarrow x_n$, it follows that x_i and x_n should also be classified to the same state. That is, vectors $\boldsymbol{x}_p$ and $\boldsymbol{x}_q$ are merged if they have a common element. To form vectors $\boldsymbol{x}_l, l = 1, \ldots, L$, we begin with $|\boldsymbol{X}^{\text{ex}}|$ ($|\boldsymbol{x}|$ symbolizes the number of elements in vector $\boldsymbol{x}$) initial vectors of single PD measurements, and iteratively merge vectors. This process continues until no two vectors can be merged. As a result, we reduce the problem of classifying $x_i \in \boldsymbol{X}^{\text{ex}}$ into classifying $\boldsymbol{x}_l$, which account for resolution limitations and node drifting.

While classification of measurement samples into two distinct distributions is a common problem solved by the expectation maximization (EM) algorithm (cf. [31]), here classification should also satisfy constraints (10), (9), and (11), where the latter two constraints introduce dependencies between $\boldsymbol{\omega}_1$ and $\boldsymbol{\omega}_2$. We start by formulating the log-likelihood function $L(\boldsymbol{\theta}|\boldsymbol{\theta}^p)$, where $\boldsymbol{\theta}^p$ is the vector of distribution parameters estimated in the pth iteration of the EM algorithm. Next, we formulate a constrained optimization problem to estimate parameters k_m, υ_m, σ_m and β_m that maximize $L(\boldsymbol{\theta}|\boldsymbol{\theta}^p)$, and offer a heuristic approach to efficiently solve it. Finally, given an estimation for $\boldsymbol{\theta}$, we calculate the probability of $\boldsymbol{x}_l$ belonging to class $m = 1, 2$, and classify the elements of $\boldsymbol{X}^{\text{ex}}$ accordingly.

A. Formalizing the Log-Likelihood Function

Let the random variable λ_l be the classifier of $\boldsymbol{x}_l$, such that if $\boldsymbol{x}_l$ is associated with class $m,\ m \in \{1, 2\}$, then $\lambda_l = m$. Also let $\boldsymbol{\lambda} = [\lambda_1, \ldots, \lambda_L]$. Since elements in $\boldsymbol{X}^{\text{ex}}$ are assumed

[4]For example, an anchored node often moves around the location of its anchor.

independent,

$$\Pr(\lambda_l = m|\boldsymbol{x}_l, \boldsymbol{\theta}^p) = \frac{k_m^p p(\boldsymbol{x}_l|\boldsymbol{\omega}_m^p)}{p(\boldsymbol{x}_l|\boldsymbol{\theta}^p)} = \frac{k_m^p \prod\limits_{x_i \in \boldsymbol{x}_l} p(x_i|\boldsymbol{\omega}_m^p)}{\sum_{j=1}^{2} k_j^p \prod\limits_{x_i \in \boldsymbol{x}_l} p(x_i|\boldsymbol{\omega}_j^p)} \ . \tag{16}$$

Then, we can write the expectation of the log-likelihood function with respect to the conditional distribution of $\boldsymbol{\lambda}$ given $\boldsymbol{X}^{\mathrm{ex}}$ and the current estimate $\boldsymbol{\theta}^p$ as

$$\begin{aligned} &L(\boldsymbol{\theta}|\boldsymbol{\theta}^p) = E\left[\ln\left(\Pr(\boldsymbol{X}^{\mathrm{ex}}, \boldsymbol{\lambda}|\boldsymbol{\theta})\right)|\boldsymbol{X}^{\mathrm{ex}}, \boldsymbol{\theta}^p\right] = \\ &\sum_{m=1}^{2}\left[\sum_{l=1}^{L}\Pr(\lambda_l = m|\boldsymbol{x}_l, \boldsymbol{\theta}^p)\sum_{x_i \in \boldsymbol{x}_l}\ln p(x_i|\boldsymbol{\omega}_m) + \sum_{l=1}^{L}\Pr(\lambda_l = m|\boldsymbol{x}_l, \boldsymbol{\theta}^p)\ln k_m\right] \ , \end{aligned} \tag{17}$$

where $\ln x = \log_{\mathrm{e}} x$ is the natural logarithmic function.

Assuming knowledge of $\boldsymbol{\theta}^p$, $\boldsymbol{\theta}^{p+1}$ is estimated as the vector of distribution parameters that maximizes (17) while satisfying constraints (9), (10) and (11). This procedure is repeated for P_{last} iterations, and the convergence of (17) to a local maximum is proven [31]. Then, we calculate $\Pr(\lambda_l = m|\boldsymbol{x}_l, \boldsymbol{\theta}^{P_{\mathrm{last}}})$ using (16), and associate vector $\boldsymbol{x}_l$ with the LOS path if

$$\Pr(\lambda_l = 1|\boldsymbol{x}_l, \boldsymbol{\theta}^{P_{\mathrm{last}}}) > \Pr(\lambda_l = 2|\boldsymbol{x}_l, \boldsymbol{\theta}^{P_{\mathrm{last}}}) \ , \tag{18}$$

or with an SNLOS path otherwise. Estimation $\boldsymbol{\theta}^{P_{\mathrm{last}}}$ and classifications λ_l could be used further to improve the accuracy of UWAL, e.g., [23], [26]. We observe that the two terms on the right-hand side of (17) can be separately maximized, i.e., given $\boldsymbol{\theta}^p$, we can obtain $\boldsymbol{\omega}_m^{p+1}$ from maximizing the first term, and k_m^{p+1} from maximizing the second term. Thus (see details in [31]),

$$k_m^{p+1} = \frac{1}{L}\sum_{l=1}^{L}\Pr(\lambda_l = m|\boldsymbol{x}_l, \boldsymbol{\theta}^p), \quad m = 1, 2 \ . \tag{19}$$

In the following, we describe the details of our classification procedure for the estimation of $\boldsymbol{\omega}_m$, followed by a heuristic approach for the initial estimates $\boldsymbol{\theta}^0$.

B. Estimating the Distribution Parameters $\boldsymbol{\omega}_1$ and $\boldsymbol{\omega}_2$

To estimate $\boldsymbol{\omega}_m$, we consider only the first term on the right-hand side of (17), which for the PDF (6) is given by

$$\begin{aligned} f(\upsilon_m, \sigma_m, \beta_m) \ = \ &\sum_{l=1}^{L}\sum_{x_i \in \boldsymbol{x}_l}\Pr(\lambda_l = m|\boldsymbol{x}_l, \boldsymbol{\theta}^p) \\ &\left[\ln\beta_m - \ln(2\sigma_m) - \ln\Gamma(\frac{1}{\beta_m}) - \left(\frac{|x_i - \upsilon_m|}{\sigma_m}\right)^{\beta_m}\right] \ . \end{aligned} \tag{20}$$

Then, considering constraints (9), (10) and (11), we find $\boldsymbol{\omega}_m^{p+1}$ by solving the following optimization problem:

$$\boldsymbol{\omega}_1^{p+1}, \boldsymbol{\omega}_2^{p+1} = \underset{\boldsymbol{\omega}_1, \boldsymbol{\omega}_2}{\operatorname{argmin}} \; -\sum_{m=1}^{2} f(\upsilon_m, \sigma_m, \beta_m) \tag{21a}$$

$$\text{s.t.} \; : \upsilon_1 \leq \upsilon_2 \leq \upsilon_1 + T_{\text{LIR}} \tag{21b}$$

$$\sigma_m \sqrt{\frac{\Gamma\left(\frac{3}{\beta_m}\right)}{\Gamma\left(\frac{1}{\beta_m}\right)}} - T_{\text{LIR}} \leq 0 \; , \; m = 1, 2 \tag{21c}$$

$$\sigma_1 - \sigma_2 \leq 0 \; . \tag{21d}$$

We observe that convexity of $f(\upsilon_m, \sigma_m, \beta_m)$ depends on β_m. In Appendix A, we present an alternating optimization approach (cf. [32]) to efficiently solve (21).

Next, we present an algorithm to obtain the initial estimation, $\boldsymbol{\theta}^0$, whose accuracy affects the above refinement as well as the convergence rate of the EM algorithm.

C. Forming Initial Estimation $\boldsymbol{\theta}^0$

Our algorithm to estimate $\boldsymbol{\theta}^0$ is based on identifying a single group, $\boldsymbol{x}_{l^*}$, whose elements belong to the LOS class with high probability, i.e., $\Pr(\lambda_{l^*} = 1) \approx 1$. This group is then used as a starting point for the K-means clustering algorithm [31], resulting in an initial classification λ_l for $\boldsymbol{x}_l, \; l = 1, \ldots, L$, to form two classified sets $\boldsymbol{X}_m^{\text{ex}}, \; m = 1, 2$. Finally, we evaluate the mean, variance, and kurtosis of the elements in vector $\boldsymbol{X}_m^{\text{ex}}$, denoted as $E[\boldsymbol{X}_m^{\text{ex}}]$, $\text{Var}[\boldsymbol{X}_m^{\text{ex}}]$, and $\text{Kurtosis}[\boldsymbol{X}_m^{\text{ex}}]$, respectively, to estimate $\boldsymbol{\theta}^0$ using the following properties for distribution (6):

$$\frac{|\boldsymbol{X}_m^{\text{ex}}|}{|\boldsymbol{X}^{\text{ex}}|} = k_m \; , \tag{22a}$$

$$E[\boldsymbol{X}_m^{\text{ex}}] = \upsilon_m \; , \tag{22b}$$

$$\text{Var}[\boldsymbol{X}_m^{\text{ex}}] = \frac{\sigma_m^2 \Gamma\left(\frac{3}{\beta_m}\right)}{\Gamma\left(\frac{1}{\beta_m}\right)} \; , \tag{22c}$$

$$\text{Kurtosis}[\boldsymbol{X}_m^{\text{ex}}] = \frac{\Gamma\left(\frac{5}{\beta_m}\right)\Gamma\left(\frac{1}{\beta_m}\right)}{\Gamma\left(\frac{3}{\beta_m}\right)^2} - 3 \; . \tag{22d}$$

Since we assume that $\sigma_1 < \sigma_2$ (see (9)), we expect small differences between measurements of the LOS link, compared to those of SNLOS links. We use this attribute to identify group $\boldsymbol{x}_{l^*}$

by filtering $\boldsymbol{X}^{\mathrm{ex}}$ and calculating the first derivative of the sorted filtered elements. Group $\boldsymbol{x}_{l^*}$ corresponds to the smallest filtered derivative.

D. Discussion

We note that the constraints in (21) do not set bounds on the values of $\boldsymbol{\omega}_1$ and $\boldsymbol{\omega}_2$, but rather determine the dependencies between them. This is because, apart from the value of T_{LIR} and distribution (6), we do not assume a-priori knowledge about the values of k_m and $\boldsymbol{\omega}_m,\ m = 1, 2$. In a scenario where the LOS path is always the strongest and PD measurements are all LOS-related, i.e., all elements of $\boldsymbol{X}^{\mathrm{ex}}$ belong to one class, our classifier might still estimate both k_1 and k_2 to be non-zero, resulting in wrong classification into two classes. In this case, using the average of the elements of $\boldsymbol{X}^{\mathrm{ex}}$ might give a better estimation of d_{LOS} than υ_1.

To limit this shortcoming of our classifier, we assume that υ_1 and υ_2 are distinct if $\boldsymbol{X}^{\mathrm{ex}}$ is indeed a mixture of two distributions. To this end, in the last iteration, P_{last}, we classify $\boldsymbol{X}^{\mathrm{ex}}$ as a single class (of unknown type) if the difference $|\upsilon_1^{P_{\mathrm{last}}} - \upsilon_2^{P_{\mathrm{last}}}|$ is smaller than a threshold value, $\Delta\upsilon$ (determined by the system resolution for distinct paths). Then, if required, we find the distribution parameters of the (single) class by solving a relaxed version of (21), setting $k_1 = 1$ and $k_2 = 0$. Nevertheless, we motivate relevance of our classifier in Section VI-B by showing that scenarios in which $\boldsymbol{X}^{\mathrm{ex}}$ is indeed a mixture of two distributions are not rare in real sea environments.

E. Summarizing the Operation of the Classifier

We now summarize the operation of our classification algorithm, whose pseudo-code is presented in Algorithm 1. First, we evaluate d_i^{PD} and $d_i^{\mathrm{RSS,min}}$ (lines 1-2). If $d_i^{\mathrm{RSS,min}} > d_i^{\mathrm{PD}}$, we classify x_i as ONLOS; otherwise, we classify it as non-ONLOS (lines 3-5) and form the vector of non-ONLOS PD measurements, $\boldsymbol{X}^{\mathrm{ex}}$, and groups $\boldsymbol{x}_l,\ l = 1, \ldots, L$ (line 7). Next, we form the initial solution, $\boldsymbol{\theta}_m^0$ (line 7), and run the EM algorithm for P_{last} iterations (lines 8-14). The procedure starts with estimating k_m^p (line 9), followed by an iterative procedure to estimate $\boldsymbol{\omega}_m^p$ for a pre-defined number of repetitions N_{repeat} (lines 10-13). After iteration P_{last}, we check if vector $\boldsymbol{X}^{\mathrm{ex}}$ consists of two classes (line 15), and determine classifiers $\lambda_l,\ l = 1, \ldots, L$ (line 16); otherwise $\boldsymbol{X}^{\mathrm{ex}}$ is classified as a single class (of unknown type), and, if estimating $\boldsymbol{\omega}_m$

Algorithm 1 Classifying $\boldsymbol{X}$

1: $d_i^{\mathrm{PD}} := \ c \cdot x_i$
2: Calculate $d_i^{\mathrm{RSS,min}}$ using RSS measurements, $\gamma_{\max}$, $\alpha_{\max}$ and model (2)
3: **if** $d_i^{\mathrm{RSS,min}} > d_i^{\mathrm{PD}}$ **then**
4: Classify x_i as ONLOS link
5: **else**
6: Exclude ONLOS measurements to form vector $\boldsymbol{X}^{\mathrm{ex}}$ and groups $\boldsymbol{x}_l$ satisfying (15)
7: Estimate $\boldsymbol{\theta}^0$
8: **for** $p := 2$ to P_{last} **do**
9: Calculate $k_m^p,\ m = 1, 2$ using (16) and (19)
10: **for** $i := 1$ to N_{repeat} **do** {alternating maximization to solve (21) (see Appendix A)}
11: Estimate $\boldsymbol{\omega}_m^{p,i},\ m = 1, 2$ and set $\upsilon_m^{p,i+1}$:=$\upsilon_m^{p,i}$, $\sigma_m^{p,i+1}$:=$\sigma_m^{p,i}$, $\beta_m^{p,i+1}$:=$\beta_m^{p,i}$
12: **end for**
13: $m = 1, 2$: υ_m^p:=$\upsilon_m^{p,N_{\mathrm{repeat}}}$, σ_m^p:=$\sigma_m^{p,N_{\mathrm{repeat}}}$, β_m^p:=$\beta_m^{p,N_{\mathrm{repeat}}}$
14: **end for**
15: **if** $|\upsilon_1^{P_{\mathrm{last}}} - \upsilon_2^{P_{\mathrm{last}}}| > \Delta v$ **then**
16: Calculate $\Pr(\lambda_l = m|\boldsymbol{x}_l, \boldsymbol{\theta}^{P_{\mathrm{last}}})$ and λ_l, $m = 1, 2,\ l = 1, \ldots, L$ using (16), (18)
17: **else**
18: Vector $\boldsymbol{X}^{\mathrm{ex}}$ consists of a single class. Repeat steps 7-14 for $k_1 = 1,\ k_2 = 0$
19: **end if**
20: **end if**

is required, we repeat the above procedure while setting $k_1 = 1,\ k_2 = 0$ (line 18). The software implementation of the above algorithm can be downloaded from [33].

The EM algorithm, as well as the alternating optimization process described in Appendix A, provably converge to a local maximum of the log-likelihood function (17). In the following, we provide the hybrid Cramér-Rao bound (HCRB) as a benchmark for our classifier.

F. Hybrid Cramér-Rao Bound (HCRB)

Consider the vector of measurements $\boldsymbol{X}^{\text{ex}}$ whose elements are drawn from distributions (6) with $M = 2$ classes (we assume that ONLOS measurements have correctly been identified). Our classifier estimates the vector $\boldsymbol{\theta} = [\upsilon_1, \sigma_1, \beta_1, k_1, \upsilon_2, \sigma_2, \beta_2] = [\theta_1, \ldots, \theta_7]$. We observe that constraints (11), (9), and (10), introduce dependencies between pairs (θ_1, θ_5), (θ_2, θ_6), $(\theta_r, \theta_{r+1}),\ r = 2, 6$, respectively. Thus, we cannot use the conventional Cramér-Rao Bound to lower bound the variance of any unbiased estimator of $\boldsymbol{\theta}$. Instead, we apply the HCRB considering θ_1 as a deterministic and $\boldsymbol{\theta}_r = [\theta_2, \ldots, \theta_7]$ a vector of random variables having prior distributions, respectively. The HCRB is given by [34]

$$E_{\boldsymbol{X}^{\text{ex}}, \boldsymbol{\theta}_r|\theta_1}\left[\left(\boldsymbol{\theta}^{P_{\text{last}}} - \boldsymbol{\theta}\right)\left(\boldsymbol{\theta}^{P_{\text{last}}} - \boldsymbol{\theta}\right)^T\right] \geq \text{H}^{-1}(\theta_1)\ , \tag{23}$$

where $\text{H}(\theta_1) \in \Re^{7\times 7}$ is the hybrid Fisher information matrix[5] (HFIM). Let ϱ_i be the classifier of x_i (i.e., $\varrho_i = \lambda_l$ if $x_i \in \boldsymbol{x}_l$). Then, the (j, q)th element of the HFIM is

$$\text{H}(\theta_1)_{j,q} = E_{\boldsymbol{\theta}_r|\boldsymbol{\theta}_1}\left[F(\boldsymbol{\theta}_r, \theta_1)_{j,q}\right] + E_{\boldsymbol{\theta}_r|\boldsymbol{\theta}_1}\left[-\frac{\partial^2}{\partial\theta_j\partial\theta_q}\log p(\boldsymbol{\theta}_r|\theta_1)\right]\ , \tag{24}$$

where

$$F(\boldsymbol{\theta}_r, \theta_1)_{j,q} = E_{\boldsymbol{X}^{\text{ex}}|\boldsymbol{\theta}_r, \boldsymbol{\theta}_1}\left[-\sum_{i=1}^{|\boldsymbol{X}^{\text{ex}}|}\frac{\partial^2}{\partial\theta_j\partial\theta_q}\log k_{\varrho_i} p(x_i|\boldsymbol{\omega}_{\varrho_i})\right]\ . \tag{25}$$

Solving (24) requires the calculation of

$$p(\boldsymbol{\theta}_r|\theta_1) = p(k_1)p(\upsilon_2|\upsilon_1)p(\sigma_2|\sigma_1, \beta_2)p(\sigma_1|\beta_1)p(\beta_1)p(\beta_2)\ . \tag{26}$$

Since, as discussed in Section V-D, we do not assume further knowledge about the values of k_1 and $\boldsymbol{\omega}_m,\ m = 1, 2$, accounting for constraints (7)-(11) we assume $p(\upsilon_2|\upsilon_1)$ is uniform between υ_1 and $\upsilon_1 + T_{\text{LIR}}$, $p(\sigma_2|\sigma_1, \beta_2)$ is uniform between σ_1 and $T_{\text{LIR}}\sqrt{\frac{\Gamma\left(\frac{1}{\beta_2}\right)}{\Gamma\left(\frac{3}{\beta_2}\right)}}$, $p(\sigma_1|\beta_1)$ is uniform between 0 and $T_{\text{LIR}}\sqrt{\frac{\Gamma\left(\frac{1}{\beta_1}\right)}{\Gamma\left(\frac{3}{\beta_1}\right)}}$, and $p(\beta_m),\ m = 1, 2$, is uniform between 1 and a deterministic parameter, G. Furthermore, we assume $p(k_1)$ is uniform between 0 and 1. Exact expressions for (24) are given in Appendix B. For the numerical results presented in the following section we evaluate the HCRB through Monte-Carlo simulations considering the above uniform distributions.

[5]Note that while the EM algorithm works on vectors $\boldsymbol{x}_l$, the actual inputs to our classifier are PD measurements. Thus, in forming the HCRB, we use x_i rather than $\boldsymbol{x}_l$.

VI. Performance Evaluation

In this section, we present results from both computer simulations and sea trials to demonstrate the performance of our classification algorithm. The results are presented in terms of detection probabilities of LOS, SNLOS, and ONLOS links. In addition, we measure estimation errors $|\upsilon_m^p - \upsilon_m|$, $|\sigma_m^p - \sigma_m|$, and $|\beta_m^p - \beta_m|$. We compare our results to the HCRB presented in Section V-F, as well as to several benchmark methods. The purpose of the simulations is to evaluate the performance of our classifier in a controlled environment, while results from sea-trial measurements reflect performance in actual UWACs.

A. Simulations

Our simulation setting includes a Monte-Carlo set of 10000 channel realizations, where two time-synchronized nodes, uniformly randomly placed into a square area of 1 km, exchange packets. The setting includes two horizonal and two vertical obstacles of length 20 m, also uniformly randomly placed into the square area, such that a LOS always exists between the two nodes. In each simulation, we consider a packet of 200 symbols of duration $T_s = 10$ msec and bandwidth $B = 6$ kHz transmitted at a propagation speed of $c = 1500$ m/sec. To model movement in the channel (dealt with by forming groups $\boldsymbol{x}_l$), during packet reception the two nodes move away from each other at constant relative speed of 1 m/sec, and $d_{\rm LOS}$ is considered as the LOS distance between the nodes when the 100th symbol arrives.

In our simulations, we use model (1) to obtain set $\boldsymbol{X}$ as follows. For each channel realization and node positions, we find the LOS distance between the two nodes, and determine $\upsilon_1 = x_{\rm LOS}$. Based on the position of nodes and obstacles, we identify ONLOS links as single reflections from obstacles and determine υ_3 as the average delay of the found ONLOS links. We use $T_{\rm LIR} = 0.1$ sec and based on constraint (11), we randomize υ_2 according to a uniform distribution between υ_1 and $\upsilon_1 + T_{\rm LIR}$. For the other distribution parameters $\boldsymbol{\theta}$, we determine $\beta_m,\ m = 1, 2, 3$ as an integer between 1 and 6 with equal probability (i.e., $G = 6$ in (26)), and $\sigma_m,\ m = 1, 2, 3$ according to (8) with ς_m uniformly distributed between 0 and $(T_{\rm LIR})^2$, preserving $\varsigma_1 < \varsigma_2$. Based on model (5), we then randomize $x_i,\ i = 1, \ldots, 200$ using distribution (6) and a uniformly distributed $k_m,\ m = 1, 2, 3$ between 0 and 1, while keeping $\sum_{m=1}^{3} k_m = 1$ and setting $k_3 = 0$ if no ONLOS link is identified. Considering the discussion in Section V-D, we use $\Delta v = \frac{1 \text{ m}}{c}$ as a detection threshold to check if measurements in vector $\boldsymbol{X}^{\rm ex}$ correspond to a single link.

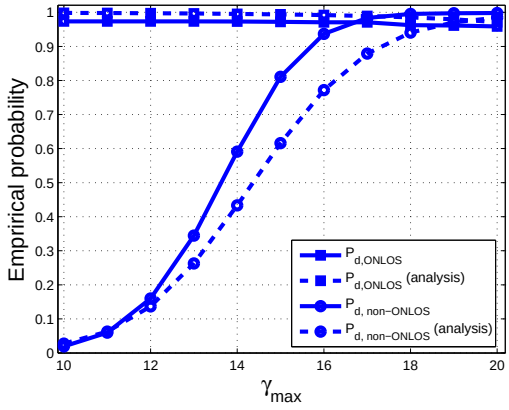

Fig. 2: $\Pr_{\mathrm{d,non-ONLOS}}$ and $\Pr_{\mathrm{d,ONLOS}}$ vs. $\gamma_{\max}$. $\gamma = 15$, $\alpha = 1.5$.

Additionally, for forming groups $\boldsymbol{x}_l$ (see (15)), we use an assumed coherence time $\tilde{T}_c = a \cdot T_s$, where $a \in \{1, 5, 10\}$, and a quantization threshold $\Delta T = 0.16$ msec based on the bandwidth of the transmitted signals. Note that since the distance between nodes changed by 2 m during reception of the 200 symbols, if $a > \frac{2\text{ m}}{\Delta T \cdot c} \approx 8.3$, condition (15b) is irrelevant, whereas $a = 1$ results into single-element vectors $\boldsymbol{x}_l$.

To simulate channel attenuation (2), we use $\gamma = 15$, $\alpha = 1.5$ dB/km (considering a carrier frequency of 15 kHz [27]), and set ϵ to be zero-mean Gaussian with variance $5/\mathrm{dB}^2$//μPa@1m. We use a source power level of 100 dB//μPa@1m and a zero-mean Gaussian ambient noise with power 20 dB//μPa@1m, such that the signal-to-noise ratio (SNR) at the output of the channel is high. Attenuation in LOS and SNLOS links is determined based on (2), while for ONLOS links we use (3) and set $\mathrm{RL} = 10$ dB//μPa@1m. To obtain the lower bound on RSS-based distance, $d_i^{\mathrm{RSS,min}}$, $i = 1, \ldots, 200$, we use the attenuation model in (2) with $\gamma_{\max} = 20$ and $\alpha_{\max} = 2$ dB/km. An implementation of the simulation environment can be downloaded from [33].

First, in Figure 2 we show empirical detection probabilities for ONLOS and non-ONLOS links as a function of $\gamma_{\max}$, as well as corresponding results using bounds (14) and (13). We observe a good match between the empirical results and the analytical bound for $\Pr^{\mathrm{d,ONLOS}}$, and that $\Pr^{\mathrm{d,ONLOS}}$ is hardly affected by $\gamma_{\max}$. However, $\Pr^{\mathrm{d,non-ONLOS}}$ increases dramatically with $\gamma_{\max}$, and the corresponding bound in (13) is less tight. This is because choosing $\gamma_{\max} < \gamma$ might lead to $d^{\mathrm{RSS,min}} > d_{\mathrm{LOS}}$ and neglectance of α in (13) causes analytical inaccuracies. For

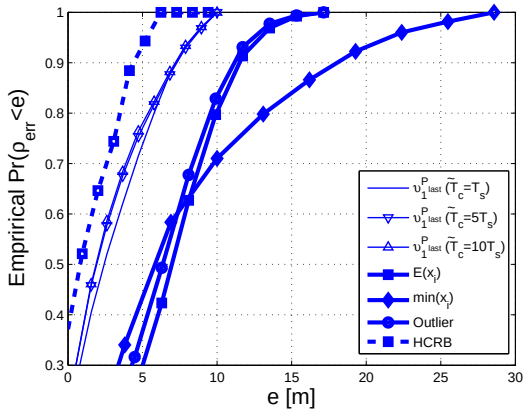

Fig. 3: Empirical C-CDF of ρ^{err} from (27).

$\Pr^{\text{d,ONLOS}}$, however, the large RL is more significant than the effect of $\gamma_{\max}$.

In Figure 3, we show the empirical complimentary cumulative distribution(C-CDF) of

$$\rho^{\text{err}} = |c\hat{x} - d_{\text{LOS}}| \ , \tag{27}$$

where $\hat{x}$ is i) $\upsilon_1^{P_{\text{last}}}$, ii) the average of the elements in $\boldsymbol{X}$ ($E(x_i)$), iii) the minimum of $\boldsymbol{X}$ ($\min(x_i)$), or iv) the average value of $\boldsymbol{X}$ after removal of outliers, as suggested in [23] (*Outlier*). Results for $\hat{x} = \upsilon_1^{P_{\text{last}}}$ are shown for $\tilde{T}_c \in \{T_s, 5T_s, 10T_s\}$. The results in Figure 3 are also compared with the HCRB presented in Section V-F. We observe that the Outlier method outperforms the naive approaches of using the average or minimum value of $\boldsymbol{X}$, where the latter performs extremely poorly for large values of ρ^{err}. However, the use of our classifier improves results significantly. For example, the proposed classifier achieves $\rho^{\text{err}} \leq 7$ m in 90% of the cases, compared to 11.2 m when using the Outlier method, and the results are close to the HCRB. Such an improvement immediately translates into better localization performance as PD estimation errors significantly decrease. Comparing results for different values of $\tilde{T}_c$, we observe that using equivalence constraints (i.e., $\tilde{T}_c > T_s$), performance slightly improves compared to the case of $\tilde{T}_c = T_s$. However, a tradeoff is observed as results for $\tilde{T}_c = 5T_s$ are marginally better than for $\tilde{T}_c = 10T_s$. This is because of erroneous assignments to vectors $\boldsymbol{x}_l$ for over-estimated coherence time, $\tilde{T}_c$. This effect becomes more significant when in addition to node movements also the channel changes (which is not included in the simulations), as we show for sea-trial performance results further below.

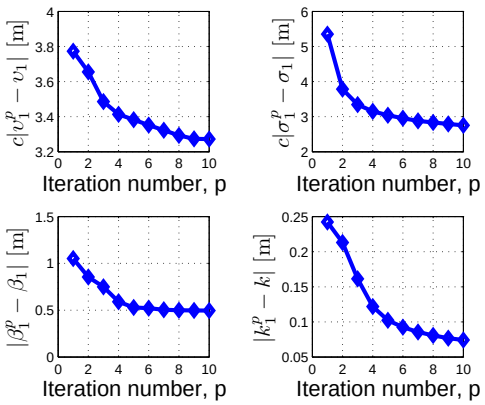

Fig. 4: Estimation error of LOS and SNLOS distribution parameters as a function of EM iteration number.

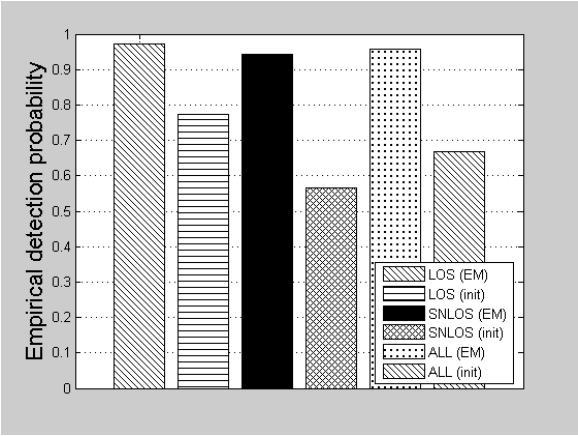

Fig. 5: Empirical detection probabilities with and without EM algorithm.

Convergence of the EM iterative procedure is demonstrated in Figure 4, where we show average estimation errors of the distribution parameters of the LOS class as a function of the EM iteration step number. We observe that estimates stabilize after 10 iteration. While improvement compared to the initialization process (see Section V-C) is shown for all estimations, the impact of the EM algorithm is most pronounced for the estimation of k_1, which greatly affect classification performance. This improvement is also observed in Figure 5, where we show empirical detection

probabilities[6] for LOS (*LOS (EM)*) and SNLOS (*SNLOS (EM)*) links, as well as the total detection probability (*ALL (EM)*), which is calculated as the rate of correct classification (of any link). Also shown are classification performance using only the initialization process (*init*), i.e., before the EM algorithm is employed. We observe that the constrained EM algorithm achieves a significant performance gain compared to the K-means algorithm, used in the initialization process. Furthermore, results show that for the former, the detection rate is more than 92% for both LOS and SNLOS.

Next, we present classification results based on real-world data collected from sea trials.

B. Sea Trials

While our simulations demonstrate good classification performance for our algorithm, the tests relied on the distribution model (6), and upper bound on transmission loss models (2) and (3), which might not be faithful representations of realistic UWACs and PD estimators. Thus, we present classification results for UWACs measured during three sea trials conducted in Israel and Singapore. One of these experiments was conducted in a harbor environment to test only ONLOS classification, while the other two were in shallow water to test LOS and SNLOS classification.

To acquire PD measurements from recorded sea-trial data, we used a matched-filter (MF) as well as the phase-only-correlator (POC) detector as described in [10]. The MF estimation method assumes an impulse-like auto-correlation of the transmitted symbols, which is not required for the POC method. However, the latter introduces some degree of noise enhancement [10]. For the ith received signal, x_i is estimated as the first peak at the output of the POC or MF that passes a detection threshold.

1) Classifying ONLOS links:

In this section, we show the performance of ONLOS link identification for an experiment conducted at the Haifa harbor, Israel, in May 2009. The experiment included four vessels, each representing an individual node in the network. Here we consider a subset of the recorded data for which nodes were static. In each vessel, a transceiver was deployed at a fixed depth of 3 m. The four nodes were time synchronized using GPS and transmitted with equal transmission power at

[6]We note that detection probabilities are calculated only when vector $\boldsymbol{X}$ consists of both LOS and SNLOS related PD measurements; classification cannot be made otherwise.

Fig. 6: Satellite picture of the sea trial location for identification of ONLOS links (picture taken from Google maps on September 29, 2009.).

a carrier frequency of 15 kHz. Referring to Figure 6, node 2 was placed at a fixed location $2A$, while nodes 1, 3 and 4 sent packets to node 2 while moving between various locations, creating a controlled environment of five non-ONLOS and four ONLOS communication links with a maximum transmission distance of 1500 m. For each link, $(2, j)$, $j \in \{1,3,4\}$, we evaluated (i) d^{PD} as the product of an assumed propagation speed of 1550 m/sec and the position of the first peak of the POC for the synchronization signal of each received packet, and (ii) $d^{\mathrm{RSS,min}}$, employing an energy detector over the synchronization signal and using (2) for $\alpha_{\max} = 2$ db/km and $\gamma_{\max} = 20$. We note that results only changed slightly when alternative methods for obtaining $d^{\mathrm{RSS,min}}$ and d^{PD} were applied.

In Table II, we present values of $d^{\mathrm{RSS,min}}$ and d^{PD} for each of the 9 communication links. Applying our proposed ONLOS link identification method, all four ONLOS links were correctly classified and there was no false classification of non-ONLOS links. In particular, we observe that for all ONLOS links, d^{PD} is much lower than $d^{\mathrm{RSS,min}}$, validating our assumption that the reflection loss of the reflecting objects (which could have been harbor docks, ship hulls, etc.) are sufficiently high to satisfy assumption (4).

2) Classifying non-ONLOS links: Next, we present results from two separate experiments conducted in open sea: (i) the first along the shores of Haifa, Israel, in August 2010 and (ii) the second in the Singapore straits in November 2011, with water depths of 40 m and 15 m respectively. This is done to demonstrate our classifier's performance in different sea environments. As

TABLE II: Harbor trial results for ONLOS link classification.

non-ONLOS links		
Link	$d^{\mathrm{RSS,min}}$ [m]	d^{PD} [m]
$(2A, 3B)$	579	780
$(2A, 4A)$	179	242
$(2A, 4B)$	343	415
$(2A, 1A)$	428	610
$(2A, 3A)$	647	817
ONLOS links		
Link	$d^{\mathrm{RSS,min}}$ [m]	d^{PD} [m]
$(2A, 1B)$	1957	1105
$(2A, 3C)$	1639	740
$(2A, 1D)$	1549	1254
$(2A, 1C)$	1816	950

communication links were all non-ONLOS links in both experiments, $\boldsymbol{X}^{\mathrm{ex}} = \boldsymbol{X}$ and we only present results for LOS/SNLOS classification.

The first sea trial included three vessels, representing three mobile nodes, which drifted with the ocean current at a maximum speed of 1 m/sec, and were time-synchronized using a method described in [35]. Throughout the experiment, the node locations were measured using GPS receivers, and the sound speed was measured to be $c = 1550$ m/sec with deviations of no more than 2 m/sec across the water column. Each node was equipped with a transceiver, deployed at 10 meters depth, and transmitted more than 100 data packets which were received by the other two nodes. Each packet consisted of 200 direct-sequence-spread-sequence (DSSS) symbols of duration $T_s = 10$ msec and a spreading sequence of 63 chips was used. From each packet, vector $\boldsymbol{X}$ was obtained by applying (i) the MF detector, and (ii) the POC detector for the ith DSSS symbol.

As discussed in Section V-D, our classifier can classify $x_i \in \boldsymbol{X}^{\mathrm{ex}}$ to LOS or SNLOS only if $\boldsymbol{X}^{\mathrm{ex}}$ comprises both classes (but parameter estimation is not limited to this condition). To evaluate the likelihood for the occurrence of a single class in $\boldsymbol{X}^{\mathrm{ex}}$, we measure the difference $\rho^{\mathrm{diff}} = c(\upsilon_2^{P_{\mathrm{last}}} - \upsilon_1^{P_{\mathrm{last}}})$, assumed to be limited by node motions if $\boldsymbol{X}^{\mathrm{ex}}$ consists only of one class. Let s be the maximum node speed during the trial. By taking the first N_{sym} PD measurements

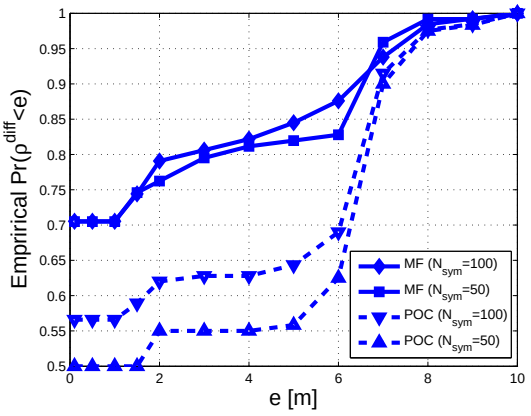

Fig. 7: Empirical C-CDF of ρ^{diff}, using POC and MF detector. $\tilde{T}_c = 10T_s$.

from each packet, the case of $\rho^{\text{diff}} > 2sN_{\text{sym}}T_s$ indicates that $\boldsymbol{X}^{\text{ex}}$ comprises two classes with high probability, and $\rho^{\text{diff}} = 0$ refers to the case where the classifier identified only one class (i.e., $|\upsilon_1^{P_{\text{last}}} - \upsilon_2^{P_{\text{last}}}| < \Delta v$ in line 15 in Algorithm 1). In Figure 7 we show the empirical C-CDF of ρ^{diff} for $N_{\text{sym}} = 50, 100$, where $\tilde{T}_c = 10T_s$. For $s = 1$ m/sec, we observe that the number of cases where $\rho^{\text{diff}} > 2sN_{\text{sym}}T_s$ is greater for the POC compared to the MF detector. This is because the auto-correlation function of the used DSSS sequence is not sufficiently narrow, which decreases the path separation in the MF compared to the POC method. From Figure 7, we further observe that for both values of N_{sym}, $\rho^{\text{diff}} > 2sN_{\text{sym}}T_s$ in more than 20% (MF) and 37% (POC) of the received packets, respectively, which motivates the use of our classifier for realistic sea environments even for short messages.

An estimation parameter of interest is $\beta_m^{P_{\text{last}}}$, which determines the type of distribution of the m^{th} class. We consider only packets received for which $\rho^{\text{diff}} > 2N_{\text{sym}}T_s$, i.e., vector $\boldsymbol{X}$ consists of two classes, and show results only for the POC method (while noting that similar results are obtained using the MF method). In Figure 8, for $N_{\text{sym}} = 100$, we show the histogram of $\beta_1^{P_{\text{last}}}$ and $\beta_2^{P_{\text{last}}}$ for different values of $\tilde{T}_c$. As the results are similar for both $\tilde{T}_c = T_s$ and $\tilde{T}_c = 10T_s$, this implies that clustering PD measurements in vectors $\boldsymbol{x}_l$ does not affect the estimated type of distribution. We also observe that the LOS class seems to lean towards $\beta_1^{P_{\text{last}}} = 6$, which implies a uniform distribution, while SNLOS measurements cluster around $\beta_2^{P_{\text{last}}} = 2$, which corresponds to the normal distribution.

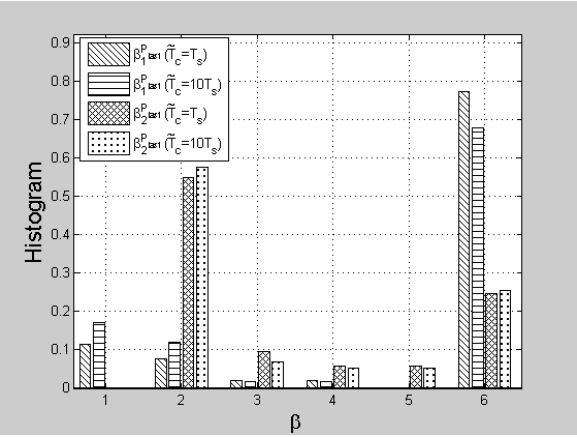

Fig. 8: Histogram of estimations $\beta_m^{P_{\text{last}}},\ m=1,2$, using POC. $N_{\text{sym}}=100$.

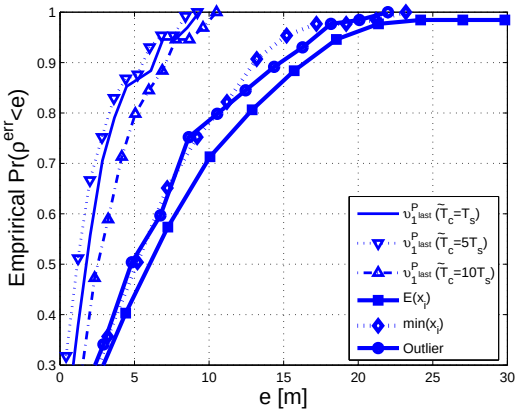

Fig. 9: Empirical C-CDF of ρ^{err} from (28), using the POC method. $\tilde{T}_c=10T_s$, $N_{\text{sym}}=100$.

In Figure 9, we show the empirical C-CDF of

$$\rho^{\text{err}}=\left|c\hat{x}-E(d_i)\right|, \tag{28}$$

where $E(d_i)$ is the mean of the GPS-based transmitter-receiver distance during the reception of each packet, $\hat{x}$ is either $\upsilon_1^{P_{\text{last}}}$, the average of the PD measurement in $\boldsymbol{X}$ ($E(x_i)$), the minimum of $\boldsymbol{X}$ ($\min(x_i)$), or the average of the obtained PD measurements after removal of outliers, i.e., the method described in [23] (*Outlier*), and elements $x_i\in\boldsymbol{X}$ were estimated using the POC method. Results are shown for $\tilde{T}_c=aT_s$, where $a\in\{1,10,20\}$. Assuming GPS location uncertainties of 5 m, we require ρ^{err} to be below 6 m. Results show that ρ^{err} for $\hat{x}=\min(x_i)$ is lower than for $\hat{x}=E(x_i)$ and almost the same as the results for the Outlier method. However, proposed

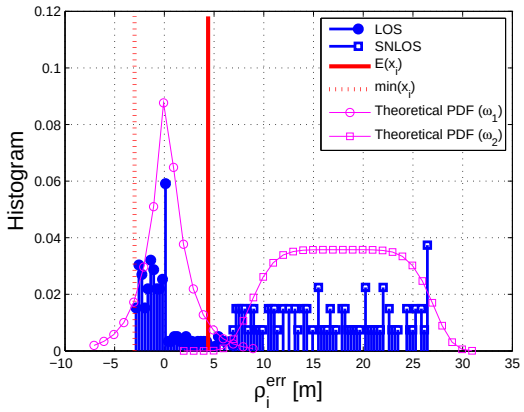

Fig. 10: Histogram of ρ_i^{err} from (29). Bin width 0.3 m, $E(d_i) = 324.1$ m.

classifier achieves always the lowest error, which is smaller than 6 m in more than 90% of the cases (compared to 55% for $\hat{x} = \min(x_i)$). Comparing results for the different values of $\tilde{T}_c$, we observe that a notable advantage for $\tilde{T}_c = 5T_s$. Since in the sea trial, during packet reception nodes were almost static, this difference is due to the time varying channel conditions.

The second sea trial included two underwater acoustic modems, manufactured by Evologics GmbH, which were deployed at a depth of 5 m. One of them was suspended from a static platform and the other from a boat anchored to the sea bottom. Throughout the experiment, the boat changed its location, resulting in three different transmitter-receiver distances which were monitored using GPS measurements. Measurements $x_i \in \boldsymbol{X}$ were obtained every 6 sec. For each transmission distance, the boat remained static for 20 min, allowing around 200 measurements x_i at each node. In this experiment, a propagation speed of $c = 1540$ m/sec, as measured throughout the year in the Singapore straits [28], was considered.

In Figure 10, since in the second sea trial the boat moved around its anchor while $\boldsymbol{X}$ was obtained, we show the histogram of

$$\rho_i^{\text{err}} = cx_i - d_i \tag{29}$$

for a single vector $\boldsymbol{X}$, where d_i is the GPS-based transmitter-receiver distance measured at time t_i (i.e., when x_i is measured), with mean and variance of $E(d_i) = 324.1$ m and $\text{Var}(d_i) = 3$ m^2, respectively. We also plotted $cE(x_i) - E(d_i)$ and $c\min(x_i) - E(d_i)$ as well as PDFs (6) of the LOS and SNLOS classes for estimation $\boldsymbol{\theta}^{P_{\text{last}}}$, for which $c\upsilon_1^{P_{\text{last}}} - E(d_i) = 0.1$ m and

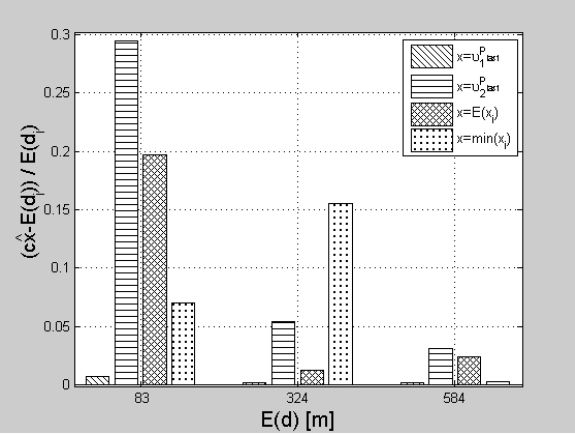

Fig. 11: $\frac{c\hat{x}-E(d_i)}{E(d_i)}$, averaged over results from the two nodes.

$cv_2^{P_{\text{last}}} - E(d_i) = 18.4$ m. The estimated factors for each class were $\beta_1^{P_{\text{last}}} = 1$ and $\beta_2^{P_{\text{last}}} = 6$, where the former matches the narrow peak distribution observed for the LOS class, and the latter matches the near uniform distribution observed for the SNLOS class. We note the good fit between the shape of the estimated PDF and the histogram for both classes. In addition, we observe that estimation $v_1^{P_{\text{last}}}$ gives much better results than the naive approach of taking the average or minimum value of $\boldsymbol{X}$.

In Figure 11 we plot the ratio $\frac{c\hat{x}-E(d_i)}{E(d_i)}$ for the three locations of the boat in the sea trial, averaged for the two nodes, for $\hat{x} = v_1^{P_{\text{last}}}, v_2^{P_{\text{last}}}, E(x_i), \min(x_i)$. The difference between results for $v_1^{P_{\text{last}}}$ and $v_2^{P_{\text{last}}}$ indicates the long channel impulse response. We observe that $\min(x_i)$ usually, but not always, results in better propagation delay estimation than $E(x_i)$, which in turn always results in better estimation than $v_2^{P_{\text{last}}}$, as expected. However, best results are obtained for $\frac{cv_1^{P_{\text{last}}}-E(d_i)}{E(d_i)}$ with average of 0.7 m compared to more than 10 m for the other methods.

Based on the results obtained from both sea trials, we conclude that our classifier significantly improves PD-based range estimations in different sea environments compared to often used conventional approaches.

VII. Conclusions

In this paper, we considered the problem of classifying propagation delay (PD) measurements in the underwater acoustic channel into three classes: line-of-sight (LOS), sea surface- or bottom-based reflections (SNLOS), and object-based reflections (ONLOS), which is important

for reducing possible errors in PD-based range estimation for underwater acoustic localization (UWAL). We presented a two-step classifier which first compares PD-based and received signal strength based ranging to identify ONLOS links, and then, for non-ONLOS links, classifies PD measurements into LOS and SNLOS paths, using a constrained expectation maximization algorithm. We also offered a heuristic approach to efficiently maximize the log-likelihood function, and formalized the Cramér-Rao Bound to validate the performance of our method using numerical evaluation. As our classifier relies on the use of simplified models, alongside simulations, we presented results from three sea trials conducted in different sea environments. Both our simulation and sea trial results confirmed that our classifier can successfully distinguish between ONLOS and non-ONLOS links, and is able to accurately classify PD measurements into LOS and SNLOS paths. Further work will include using these classifications to improve the accuracy of UWAL.

REFERENCES

[1] P. Casari and M. Zorzi, "Protocol design issues in underwater acoustic networks," *Elsevier Computer Communications*, vol. 34, no. 17, pp. 2013–2025, Nov. 2011.

[2] H. Tan, R. Diamant, W. Seah, and M. Waldmeyer, "A survey of techniques and challenges in underwater localization," in *Elsevier Journal of Ocean Engineering*, vol. 38, no. 14-15, October 2011, pp. 1663–1676.

[3] X. Cheng, H. Shu, Q. Liang, and D. Du, "Silent Positioning in Underwater Acoustic Sensor Networks," *IEEE Trans. Veh. Technol.*, vol. 57, no. 3, pp. 1756–1766, May 2008.

[4] Z. Zhou, J. H. Cui, and S. Zhou, "Efficient Localization for Large-Scale Underwater Sensor Networks," *Ad Hoc Networks*, vol. 8, no. 3, pp. 267–279, May 2010.

[5] W. Cheng, A. Y. Teymorian, L. Ma, X. Cheng, X. Lu, and Z. Lu, "3D Underwater Sensor Network Localization," *IEEE Trans. on Mobile Computing*, vol. 8, no. 12, pp. 1610–1621, December 2009.

[6] M. Stojanovic and J. G. Proakis, *Acoustic (underwater) Communications in Encyclopedia of Telecommunications*. Hoboken, NJ, USA: John Wiley and Sons, 2003.

[7] R. Diamant and L. Chorev, "Emulation system for underwater acoustic channel," in *International Undersea Defence Technology Europe conference (UDT)*, Amsterdam, the Netherlands, Jun. 2005.

[8] F. de Lima and C. Furukawa, "Development and testing of an acoustic positioning system - description and signal processing," in *IEEE Ultrasonics Symposium, 2002*, vol. 1, Oct. 2002, pp. 849–852.

[9] S. Gezci, "A survey on wireless position estimation," *Wireless Personal Communications*, vol. 44, no. 3, pp. 263–282, Feb. 2008.

[10] Z. Zhang, C. L. Law, and Y. L. Guan, "Modified phase-only correlator with kurtosis-based amplified-noise suppression," *IEEE Trans. Wireless Commun.*, vol. 9, no. 11, pp. 3341–3345, Nov. 2010.

[11] M. Dashti, M. Ghoraishi, K. Haneda, and J. Takada, "Sources of TOA estimation error in LOS scenario," in *IEEE International Conference on Ultra-Wideband (ICUWB)*, Nanjing, China, Sep. 2010.

[12] Z. N. Low, J. H. Cheong, C. L. Law, W. T. Ng, and Y. J. Lee, "Pulse detection algorithm for line-of-sight (los) uwb ranging applications," *IEEE Antennas Wireless Propagat. Lett.*, vol. 4, pp. 63–67, Nov. 2005.

[13] L. Mu, G. Kuo, and N. Tao, "A novel ToA location algorithm using LOS range estimation for NLOS environments," in *Proc. of the IEEE Vehicular Technology Conference (VTC)*, Melbourne, Australia, May 2006, pp. 594–598.

[14] J. Ash and R. Moses, "Acoustic time delay estimation and sensor network self-localization: Experimental results," *Journal of Acoustic Society of America*, vol. 118, no. 2, pp. 841–850, August 2005.

[15] D. McCrady, L. Doyle, H. Forstrom, T. Dempsey, and M. Martorana, "Mobile ranging using low-accuracy clocks," *IEEE Trans. Microwave Theory and Techniques*, vol. 48, no. 6, pp. 951–957, June 2000.

[16] S. Fischer, H. Grubeck, A. Kangas, H. Koorapaty, E. Larsson, and P. Lundqvist, "Time of arrival estimation of narrowband TDMA signals for mobile positioning," *Proc. of the IEEE International Symposium on Personal, Indoor and Mobile Radio Communications (PIMRC)*, pp. 451–455, September 1998.

[17] A. A. Saleh and R. A. Valenzuela, "A Statistical Model for Indoor Multipath Propagation," *IEEE Journal on Selected Areas in Communications*, vol. 5, no. 2, pp. 128–137, February 1987.

[18] A. J. Weiss, "Composite bound on arrival time estimation errors," *IEEE Transactions on Aerospace and Electronic Systems*, vol. 22, pp. 751–756, November 1986.

[19] Y. Zhang and L. Cheng, "A distributed protocol for multi-hop underwater robot positioning," *Proc. of IEEE International Conference on Robotics and Biometics (ROBIO)*, pp. 480–484, August 2004.

[20] A. Savvides, H. Park, and M. Srivastava, "The bits and flops of the N-hop multilateration primitive for node localization problems," *Proc. of the ACM International Workshop on Wireless Sensor Networks and Applications*, pp. 112–121, September 2002.

[21] D. Moore, J. Leonard, D. Rus, and S. Teller, "Robust distribution network localization with noisy range measurments," *Proc. of the ACM International Conference on Embedded Networked Sensor Systems (SenSys)*, pp. 50–61, nov 2004.

[22] S. Venkatraman, J. Caffery, and H. You, "A novel ToA location algorithm using LOS range estimation for NLOS environments," *IEEE Trans. Veh. Technol.*, vol. 5, no. 53, pp. 1515–1524, Sep. 2004.

[23] J. Albowicz, A. Chen, and L. Zhang, "Recursive position estimation in sensor networks," *Proc. of the International Conference on Network Protocols (ICNP)*, pp. 35–41, November 2001.

[24] N. Priyantha, A. Chakraborty, and H. Balakrishnan, "The Cricket location-support system," *Proc. of the ACM International Conference on Mobile Computing and Networking (MOBICOM)*, pp. 32–43, August 2000.

[25] P. C. Chen, "A non-line-of-sight error mitigation algorithm in location estimation," *Proc. of the IEEE Wireless Communications and Networking Conference (WCNC)*, pp. 316–320, September 1999.

[26] L. Cong and W. Zhuang, "Non-line-of-sight error mitigation in TDoA mobile location," *Proc. of the IEEE International Conference on Global Telecommunications (GlobeCom)*, vol. 1, pp. 680–684, November 2001.

[27] W. Burdic, *Underwater Acoustic System Analysis*. Peninsula Publishing, 2002.

[28] M. A. Chitre, "A high-frequency warm shallow water acoustic communications channel model and measurements," *Acoustical Society of America*, vol. 122, pp. 2580–2586, Nov. 2007.

[29] D. Mirza and C. Schurgers, "Motion-aware self-localization for underwater networks," in *ACM International Conference on Mobile Computing and Networking (MobiCom)*, San Francisco, California, USA, Sep. 2008, pp. 51–58.

[30] M. Novey, T. Adali, and A. Roy, "A complex generalized Gaussian distribution: Characterization, generation, and estimation," *IEEE Trans. Signal Processing*, vol. 58, pp. 1427–1433, Mar. 2010.

[31] S. Kay, *Fundamentals of Statistical Signal Processing: Estimation Theory*. Englewood Cliffs, NJ: Prentice-Hall, 1993.

[32] J. Bezdek and R. Hathaway, "Some notes on alternating optimization," in *International Conference on Fuzzy Systems (AFSS)*, London, UK, 2002, pp. 288–300.

[33] R. Diamant, *MATLAB implementation code for the STSL algorithm*, 2011, http://ece.ubc.ca/∼roeed/downloads.

[34] S. Bay, B. Geller, A. Renaux, J. Barbot, and J. Brossier, "On the hybrid cramer rao bound and its application to dynamical phase estimation," *IEEE Signal Processing Lett.*, vol. 15, pp. 453–456, 2008.

[35] R. Diamant and L. Lampe, "Underwater localization with time synchronization and propagation speed uncertainties," in *IEEE Workshop on Positioning, Navigation and Communication (WPNC)*, Dresden, Germany, Apr. 2011.